Supplementary Information (SI) for ChemComm.
This journal is © The Royal Society of Chemistry 2024

ChemComm

COMMUNICATION

Supporting Information

Through Thickness Anisotropy in All Inorganic Perovskite Thin Films via Two-Step Synthesis: Implications for Voltaic Devices

Yanting Yin*[a], Laura Garcia-Quintana[a], Alexandra Chapsky[b], Marta Llusca Jane[a], Drew R Evans*[a]

[a]Future Industries Institute, University of South Australia, South Australia, Australia

[b]Faculty of Sciences, University of Adelaide, 5000, Adelaide

*Ray.Yin@unisa.edu.au; *Drew.Evans@unisa.edu.au

Experimental

Sample Preparation

Fluorine-doped tin oxide (FTO) glass substrates, 25 mm × 25 mm, were sequentially cleaned by deionized water, acetone, ethanol, isopropyl alcohol (IPA), deionized water and dried at 70 °C in air atmosphere. Then, 30 nm of ZnO (acting as charge transport layer), was deposited via magnetron sputtering onto the cleaned FTO substrates. The ZnO/FTO substrates were annealed at 400 °C during 1h to crystallise the ZnO, as it would be done to complete a solar cell and cleaned under an O_2 plasma for 25 min to remove organic contamination and enhance their wettability.[1]

$CsPbBr_3$ films were prepared in typical laboratory conditions (air atmosphere, 23 °C, 35% RH) by the two-step spin-coating method, as shown in Figure S1. For the 1M $PbBr_2$ precursor, 184 mg of $PbBr_2$ (99.9% purity from Yuri Solar), with 9.2 mg Polyethylene glycol dried powder (PEG, Mw 3,350 Da from Sigma Aldrich) in a molar ratio of 0.0055 to $PbBr_2$, were mixed in 5 mL of dimethylformamide (DMF, 99.9% from Sigma Aldrich) and stirred at 80 °C for 18 hours. 120 µL of the solution was spin-coated onto the ZnO at a speed of 2000 rpm for 30 s and annealed at 90 °C for 30 min to remove the residual DMF to crystallize a $PbBr_2$ film. After cooling down, CsBr (99.8% pure from Yuri Solar) in H_2O (Milli-Q) solution (following the method of Cao et al.[2]) at 1.2 M (sample A), 1.5 M (sample B) and 1.8 M (sample C) was spin-coated onto the $PbBr_2$ (150 µL each) at a speed of 2000 rpm for 30 s, and then annealed at 250 °C for 20 min. The obtained $CsPbBr_3$ films were washed with antisolvent-IPA to further removing the solvent residue. For analysis purposes, four replicate samples were fabricated for each of the given three conditions.

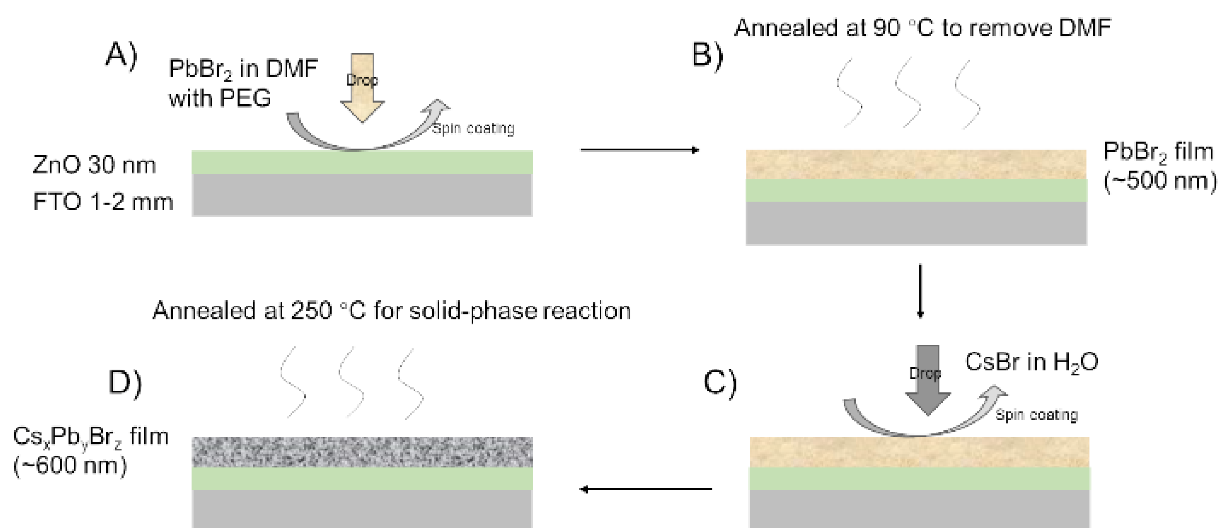

Fig. S1. *Illustration of the two-step spin coating method to form a $CsPbBr_3$ layer via $PbBr_2$ and CsBr precursors. A) $PbBr_2$ precursor was dropped onto ZnO/FTO substrates, followed by spin-coating process; B) Formed film was dried at 90 °C; C) CsBr precursor was dropped onto the $PbBr_2$ film and spin-coated; D) The film was annealed at 250 °C thus $CsPbBr_3$ was formed through solid phase reaction*

Sample Characterisation

For a preliminary characterisation of the film, the thickness of the films and relative roughness was measured by mechanical profilometry (Bruker, Dektak XT) and the morphology was qualitatively evaluated with an optical microscope (Nikon, H550S). The film thickness was measured as 612 ± 32 nm for sample A, 622 ± 22.5 nm for sample B and 626 ± 28 nm for sample C. In terms of the similarity of the thicknesses across the samples, the calculation of sputtering rate was conducted by taking the average of the film thickness (620 nm) to achieve a consistence of the three samples.
X-ray diffractometry (XRD) was conducted to analyse the structure of the $CsPbBr_3$ films. Samples were covered with Kapton tape for protection. The diffractometer was a Bruker D4 Endeavor that uses a Co-Kα source at 35 kV and at 30 mA of current. The incident angle (2Θ) ranged between 10° to 80°, with data taken at 8568 steps, 1 second exposure per step. The measurements were performed with sample spinning at 19 rpm. The facility can probe the chemical products and overall sample stoichiometry as preliminary chemical analysis. Phase changes and space groups of the crystalline structures of the samples can also be determined with a probing depth of tens of micrometres. The acquired peak positions from the analysis were compared to known reference peaks to determine the phase structure presence.

A Kratos Inc. Analytical Instrument, model AxisUltra, equipped with X-ray photoelectron spectroscopy (XPS), UV-light photoelectron spectroscopy (UPS), Ar (mono) ion source and gas cluster ion source was used to analyse the chemical an electrical property of the samples across the $Cs_xPb_yBr_z$ layers thickness. On each of the samples six spots were selected for analysis at a given depth as shown in Figure S2. Each spot was at least 4 mm away from the others to prevent the overlap of the ion source that had a spot of 2 × 2 mm. The sputtering rate of $CsPbBr_3$ was determined from a simultaneous XPS survey to observe the position of the perovskite/ZnO interface. When Zn became detectable in the XPS survey it was assumed that the perovskite/ZnO interface had been reached (assuming the thickness of the perovskite is 620 nm approximately). The etching rate of $CsPbBr_3$ was calculated to be approximately 6 nm/min.

The spots under analysis are described and listed in Table S1.

Table S1: Description of each analysis spot that is sputtered and characterised

Spot label	Sputtering duration (min)	Sputtering depth (nm)	Analysis spot description
1	0.33	2	Outermost layer
2	1	6	Surface
3	5	30	High absorption region
4	16.7	100	High absorption region
5	50	300	Middle of the film
6	103.3	620	ZnO interface

1) Spot 1 (2 nm) presents the outermost layer of the sample with a clean of surface contamination.
2) Spot 2 (6 nm) presents the surface region of the sample.
3) Spot 3 (30 nm) indicates the perovskite region that has the high optical response.[3, 4]
4) Spot 4 (100 nm) locates at the perovskite region that has the high optical response.[3]
5) Spot 5 (300 nm) presents the middle section of a perovskite film.
6) Spot 6 (620 nm) presents the end of the perovskite at the ZnO interface.

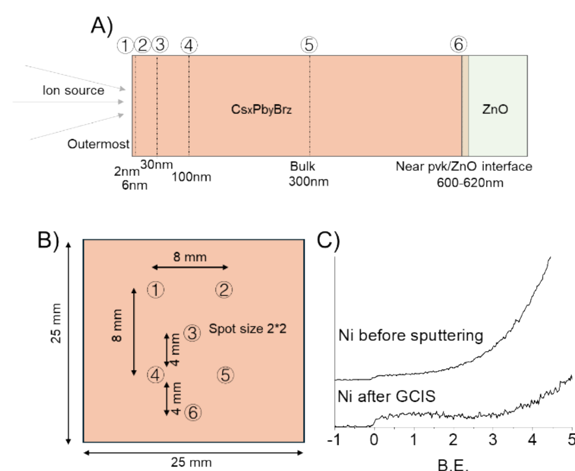

Fig S2. *A) $Cs_xPb_yBr_z$ cross-section scheme and B) Top-view of the six selected spots under analysis. C) UPS analysis of a Ni sample before and after GCIS sputtering.*

Photoelectron Spectroscopy Methodology

Ar sputtering mono atom ion source[5] (AIS) followed by Gas cluster ion source (GCIS) was executed at each of the selected spots prior to take each XPS and UPS measurement.

AIS uses a pulsed beam of Ar ions (Ar^+) with a kinetic energy of 5 keV to clean and etch the sample surface. It is a powerful technique for sample surface removal due to the high kinetic energy of the single ions. After AIS, a GCIS with a pulsed beam of 2~10 keV, distributed over a cluster of 3000+ Ar atoms, was used to further etched the $CsPbBr_3$ at a slower and gentler well-controlled removal uniformity. The GCIS was carried out with the same ion source during 30 s to eliminate any crystalline damage from the AIS technique. The UPS analysis of a Ni sample conducted with GCIS is shown in Fig S2 (C), a clear valence electron distribution indicating no obvious damage on its properties can be seen.

After the AIS and GCIS etching, XPS and UPS were performed on spots, note that not all spots were characterised with both XPS and UPS due to the representativeness of depth selection. UPS was carried out after XPS analysis thus was only conducted on spots where noticeable chemical changes were observed.

X-ray photoelectron spectroscopy (XPS) was performed to investigate the elemental composition and the chemical states of the films with an aperture size of Ø 3mm circle. The XPS instrument, uses a monochromatic X-ray source equipped with an Al anode to emit electrons onto the sample surface. The angle between the X-ray beam and the spectrometer was 54°. The

probing depth is slightly different for each element as it depends on the kinetic energy of the emitted electrons but a range of 6~10 nm can be expected. Survey spectra were recorded at a pass energy of 20 eV. High resolution spectra of C, O, Pb, Cs and Br were determined at a pass energy of 10 eV. The C-C sp3 was observed at 285.0 ± 0.2 eV[6], hence, the calibration of the spectra was not required. The measurements were carried out at ultra-high vacuum (UHV) at a base pressure of 10^{-9} mbar. The elemental concentrations of Cs, Pb and Br were derived from the peak intensity and thus were calculated and normalised with the atomic sensitive factor (ASF)[7] and relative to each other. Due to the difference in inelastic electron-mean-free-path[8] of metal and halogen, the ratio of Pb to Br or Cs to Br from XPS does not necessary represent the actual proportion. The C and O are excluded from the relative concentration calculation because they can be interfered by surface contamination.

The C 1s peak at 285.0 ± 0.15 eV[9] can be identified as representing the C-C bond, while the C-O bond peaks at 287.2 ± 0.15 eV[10]. The C=C bond can be seen at 289.2 ± 0.15 eV.[10] The O 1s spectrum of the sample can be fitted with one peak in the range of 532-532.5 eV (± 0.15 eV), contributing to C-O and C=O compositions.[11] Cs $3d_{5/2}$ peak can be identified and fitted with two individual peaks with the doublet peaks distant by 14.8 eV. The two peaks of Cs at about 724.8 ± 0.15 eV and 723.2 ± 0.15 eV can be attributed to the $CsPbBr_3$ and Cs_2PbBr_4 compounds.[12, 13] Regarding the Pb 4f peaks, the Pb $4f_{7/2}$ can be observed in the range of 136-141 eV (± 0.15 eV), while the doublet can be seen in the range of 142-147 eV (± 0.15 eV).[12, 13] Br $3d_{5/2}$ and Br $3d_{3/2}$ were observed and fitted with one peak at 68.5 ± 0.15 eV[12, 14] and 69.5 ± 0.15 eV[12, 14]. Therefore, it can be concluded that the Br did not show obvious energy shift despite the stoichiometry changes to $CsPb_2Br_5$ or Cs_2PbBr_4. The contribution from Zn at about 1022.2 ± 0.15 eV[15] is only observed when the profiling is close to the end side of the perovskite, indicating the approach to the interface. Br $3d_{5/2}$ and Br $3d_{3/2}$ were observed and fitted with one peak each; therefore, it can be concluded that the Br did not show obvious energy shift despite the stoichiometry changes to $CsPb_2Br_5$ or Cs_2PbBr_4. The contribution from Zn is only observed when the profiling is close to the bottom of the perovskite layer, indicating the underlying substrate has been reached.

Table S2: XPS peak fitting with reference

	Peak position (eV ± 0.15)	Bond assigned	Peak Assignment Reference
C 1s	284.8-285.2	C-C	9
	286.8-287.2	C-O	10
	288.8-289.2	C=C	10
O 1s	532-532.5	C-O, C=O	11
Cs 3d	723.2-725.0	$CsPbBr_3$, Cs_2PbBr_4	12, 13
	736.2-738.2	Doublet	
Pb 4f	136.0-141.0	$CsPbBr_3$	12, 13
	142.0-147.0	Doublet	
Br 3d	68.0-69.0	$CsPbBr_3$	12, 14
	70.0-71.0	Doublet	
Zn	1022.2-1023	ZnO	15

UV-light photoelectron spectroscopy (UPS) was also employed to determine the work function (WF), the valence electronic states of samples surface and the corresponding valence band maximum (VBM). A beam of UV light was projected onto the sample surface with an excitation energy of 21.2 eV, then electrons are excited and emitted from the sample surface and recorded at the detector. The approach allows to detect the states over a depth of 2.5~3 nm from the sample surface. WF can be derived from the secondary electron peak cascade while the VBM can be determined from the valence electron peak cut-off. The details can be referred to the published work and also described in simply here: 1) WF was calculated by processing a deconvolution upon the measured secondary electron peak by constructing Fermi-Dirac distribution with Gaussian fitting. The value at the energy scale where electron and hole are equally districted at the absolute zero degree condition can be taken as WF; 2) VBM was calculated at the intersection where valence electron peak shows a cut-off feature.[16] Note the conduction band edge (CB) is out of the scope of the work thus can be referred to published work.[17] Thus the bang gap (eg) can be calculated by taking the energy diversity from conduction band to valence band.

COMMUNICATION

Experimental

Morphology and Crystal Structure

In Figure S3 the morphology and the XRD results of the three $PbBr_2/CsBr$ combinations ([CsBr]: Sample A = 1.2M, B = 1.5M, and C = 1.8M) are shown. The selected concentrations were referred to Cao's work[2] that optimisation has been conducted for film quality. It can be seen the pinholes still present with the spin-coating method while the film shows crystalline structure overlaying together. The number of pinholes increases with the increasing ratio of CsBr to $PbBr_2$.

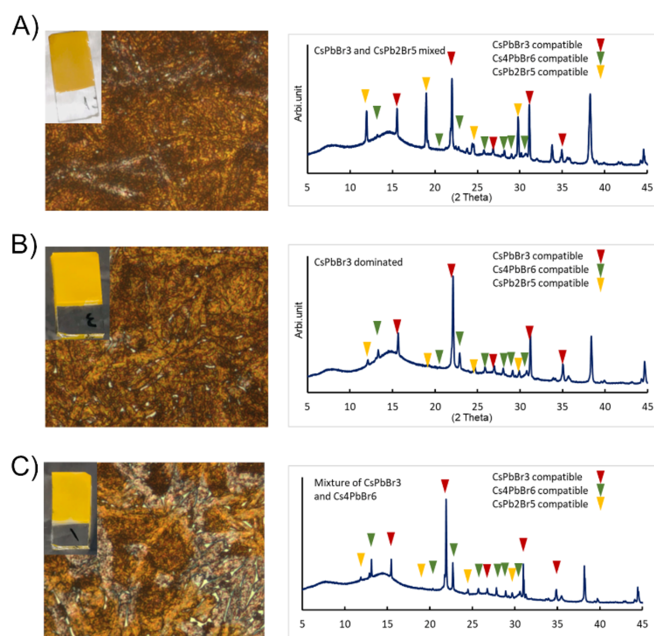

Fig S3. Optical microscopy images and X-ray diffractograms for three different chemistries by changing the concentration of CsBr precursors based on a fixed concentration of $PbBr_2$ precursor. A) 1.2M CsBr; B) 1.5M CsBr; C) 1.8M CsBr. The optical images provide qualitative assessment of the thin film uniformity and coverage. The diffractograms provide crystalline peak position assigned to crystal structure and stoichiometry.

The presence of $CsPb_2Br_5$, Cs_2PbBr_4 and $CsPbBr_3$ phases can be referred to the peak at 12°, 13.5° and 15.2°, respectively.[18] Note due to the low thickness of ZnO located at 37° and 44°[19], the glass substrate may also contribute to the peak and background. In all three samples, $CsPbBr_3$ phase dominates the film composition, while for sample A a small fraction of $CsPb_2Br_5$ and Cs_2PbBr_4 is observed. The presence of $CsPb_2Br_5$ phase increases with an increase in the $PbBr_2$ ratio to CsBr in sample B. By increasing the ratio of CsBr to $PbBr_2$ in sample C, a larger amount of Cs_2PbBr_4 phase can be identified in the film. The preliminary stoichiometry analysis indicates that the phase group of $Cs_xPb_yBr_z$ can be intentionally altered by tuning the concentration of the precursor solution. However, it is to be noted that the XRD probes several micrometres from the sample surface. Thus, the information provided is a convolution of information from several depths within the film, although the surface regions will be the majority contribution to the spectra.[20] Complementary approaches such as depth profiling analysis have been performed to further analyse the stoichiometry of the films.

XPS

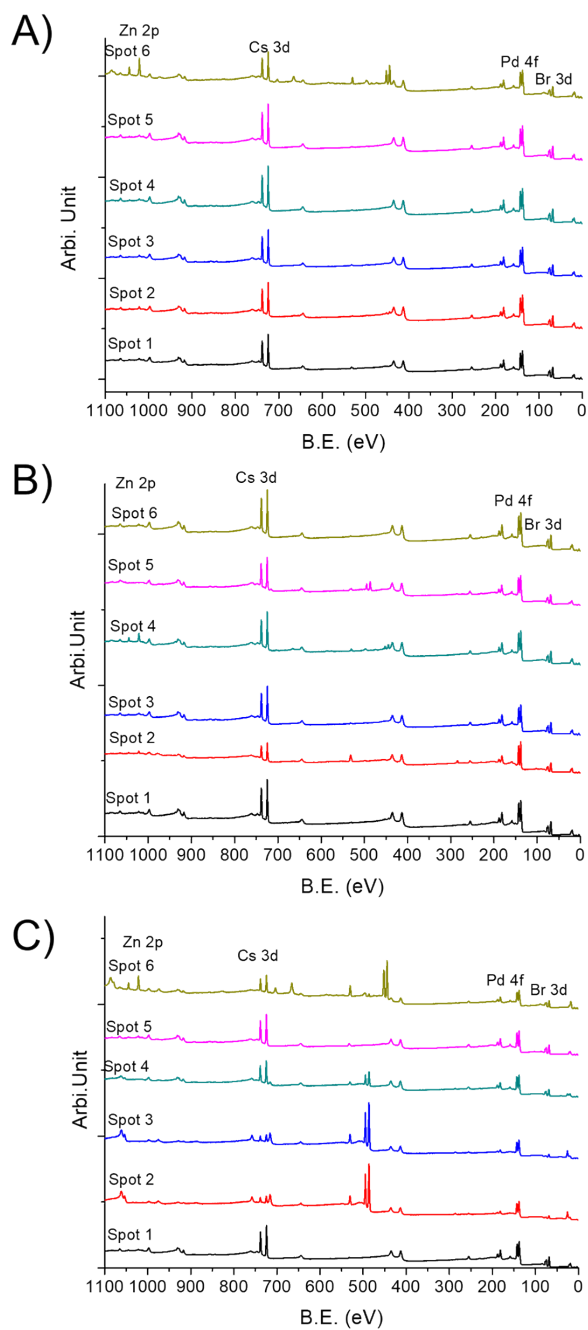

Fig S4. Survey spectra of various spots on each sample. A) Sample B with a control/balanced stoichiometry; B) Sample A with a $PbBr_2$ enriched phase; C) Sample C with CsBr enriched phase. The Zn peaks at about 1022.2 eV. Cs $3d_{5/2}$, Pb $4f_{7/2}$ and Br $3d_{5/2}$ are respectively distinguished at 725.0 eV, 138.2 eV and 68.5 eV approximately.

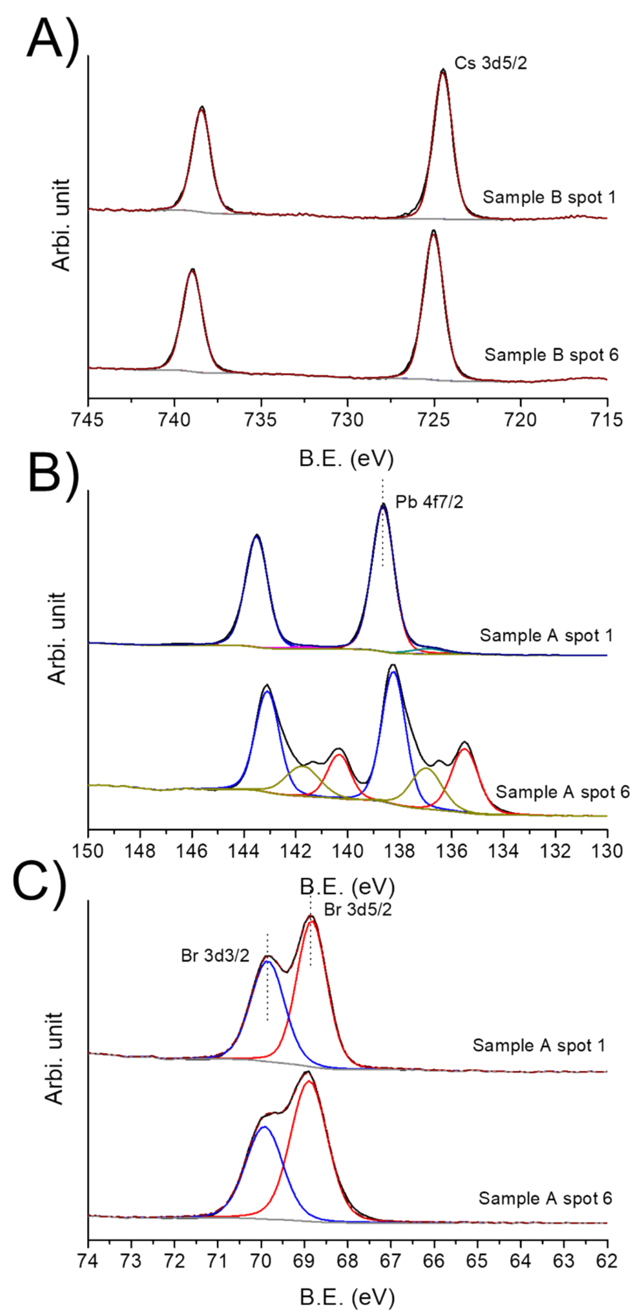

Fig S5. Example of fitting of Cs, Pb and Br of samples B, spot 1 and spot 6. Note the Cs, Pb and Br peak can be attributed to $Cs_xPb_yBr_z$. It needs to note that reduced Pb compounds can be found upon a high depth sputtering that can be attributed to sputtering damage but the nature is out of the scope of the work

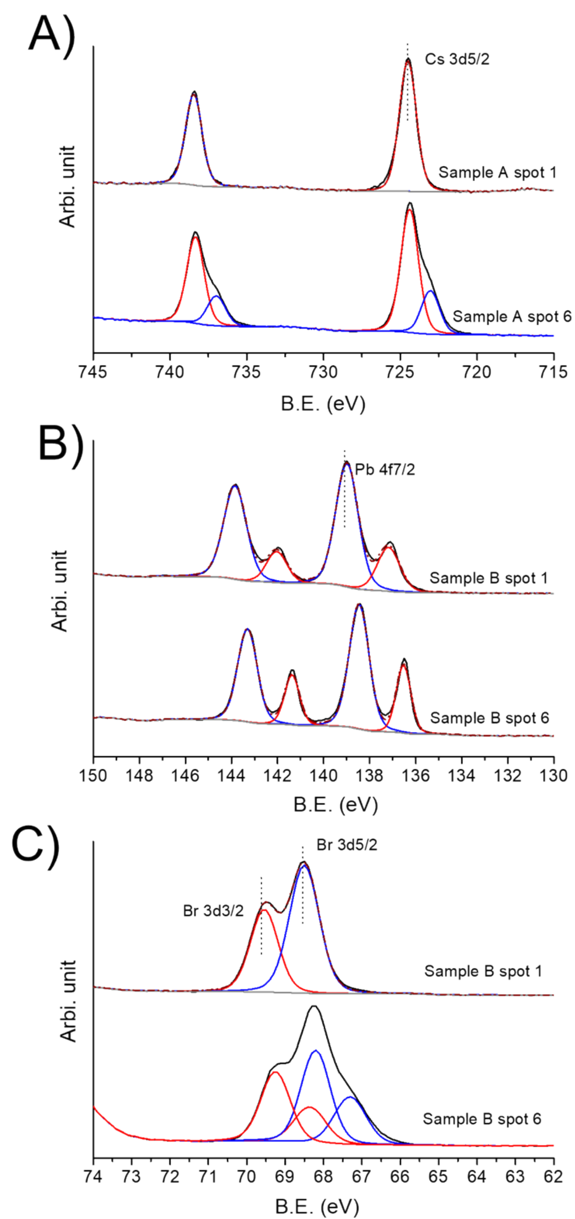

Fig S6. Example of fitting of Cs, Pb and Br of samples A, spot 1 and spot 6. Note the Cs, Pb and Br peak can be attributed to $Cs_xPb_yBr_z$. It needs to note that reduced Cs, Pb and Br compounds can be found upon a high depth sputtering that can be attributed to sputtering damage.

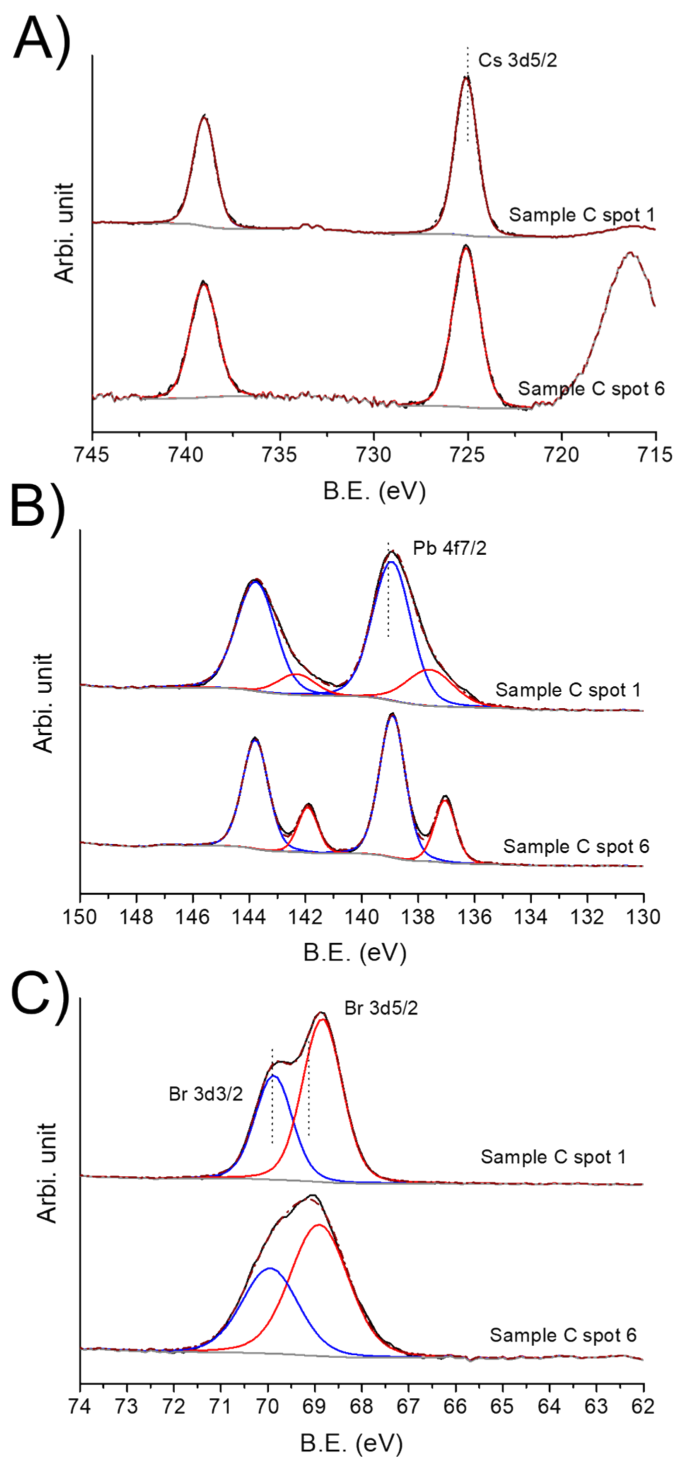

Fig S7. Example of fitting of Cs, Pb and Br of samples C, spot 1 and spot 6. Note the Cs, Pb and Br peak can be attributed to $Cs_xPb_yBr_z$. It needs to note that reduced Pb compounds can be found upon a high depth sputtering that can be attributed to sputtering damage.

UPS

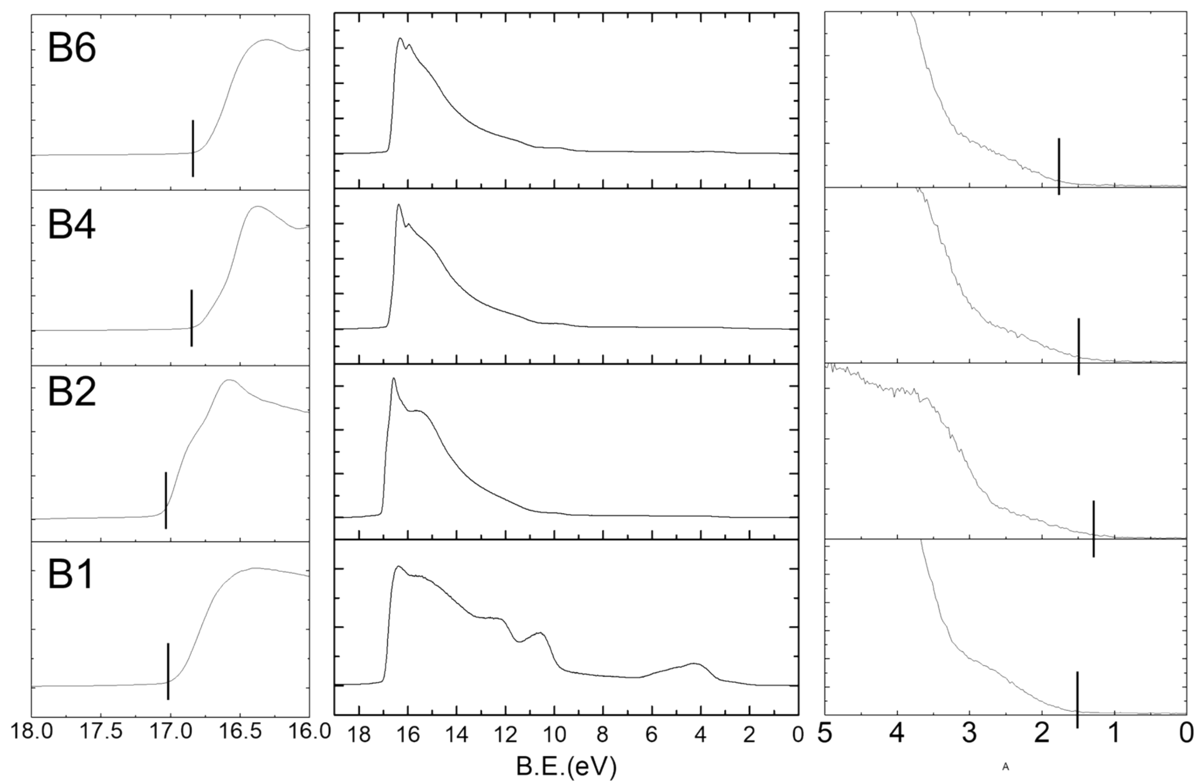

Fig S8. UPS spectra of the spot 1, 2, 4, 6 from sample B. The left figure is the magnification of region (16-18) eV where WF was calculated based on peak cut-off. The middle figure is the raw spectra. The right figure is the magnification of region (0-5) eV where valence band maximum can be calculated based on the cut-off of the valence peak.

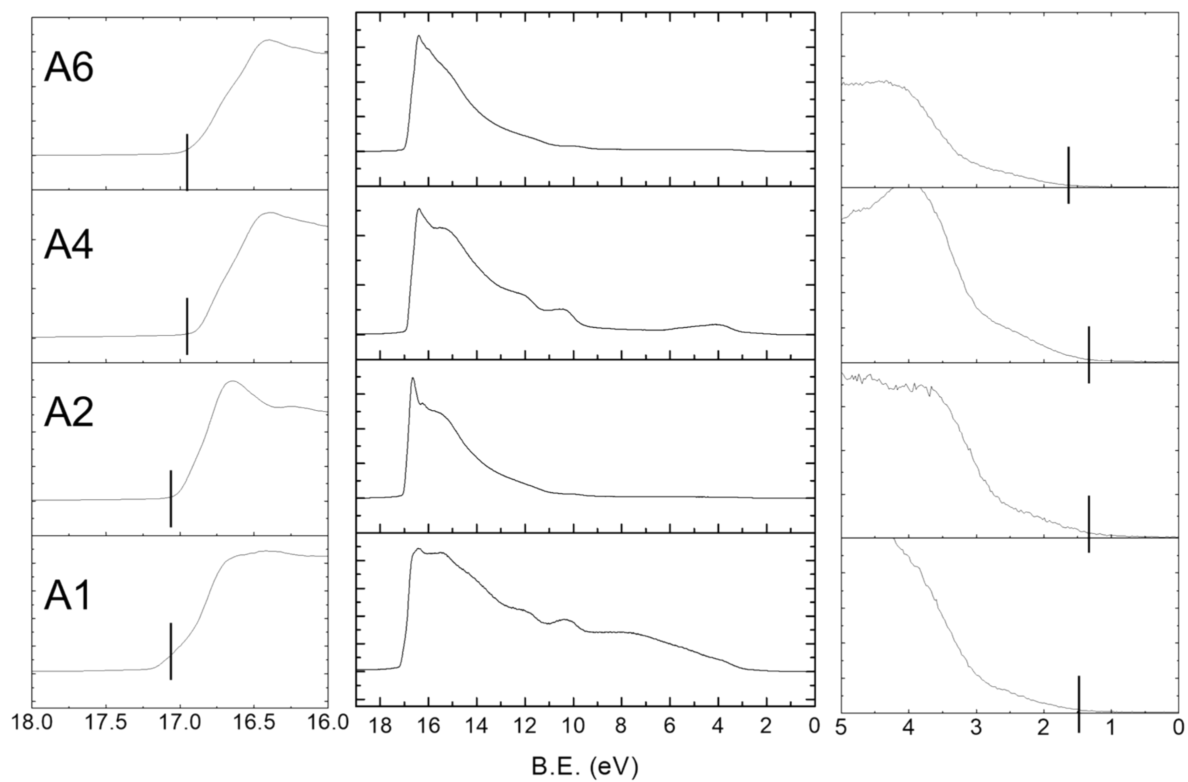

Fig S9. UPS spectra of the spot 1, 2, 4, 6 from sample A. The left figure is the magnification of region (16-18) eV where WF was calculated based on peak cut-off. The middle figure is the raw spectra. The right figure is the magnification of region (0-5) eV where valence band maximum can be calculated based on the cut-off of the valence peak.

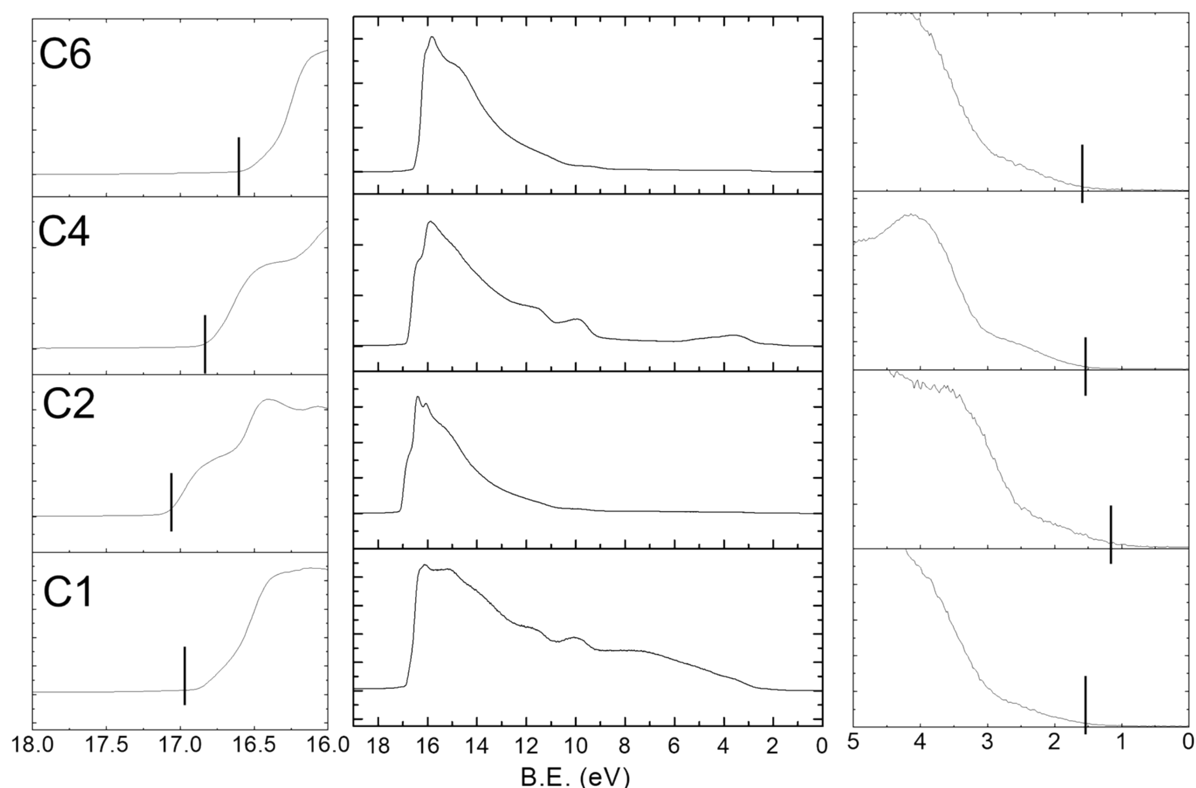

Fig S10. UPS spectra of the spot 1, 2, 4, 6 from sample C. The left figure is the magnification of region (16-18) eV where WF was calculated based on peak cut-off. The middle figure is the raw spectra. The right figure is the magnification of region (0-5) eV where valence band maximum can be calculated based on the cut-off of the valence peak.

Notes and references

1. Z. Saki, M. M. Byranvand, N. Taghavinia, M. Kedia and M. Saliba, *Energy & Environmental Science*, 2021, **14**, 5690-5722; G. Primc and M. Mozetic, *Polymers (Basel)*, 2022, **14**.
2. X. Cao, G. Zhang, L. Jiang, Y. Cai, Y. Gao, W. Yang, X. He, Q. Zeng, G. Xing, Y. Jia and J. Wei, *ACS Appl Mater Interfaces*, 2020, **12**, 5925-5931.
3. Z. Yu, H. Li, X. Shan, S. Bao, S. Psulkowski, W. Guo and T. Dickens, *Advanced Manufacturing*, 2023, DOI: 10.55092/am20230002.
4. S. M. H. Qaid, H. M. Ghaithan, B. A. Al-Asbahi and A. S. Aldwayyan, *ACS Omega*, 2021, **6**, 5297-5309.
5. R. Simpson, R. G. White, J. F. Watts and M. A. Baker, *Applied Surface Science*, 2017, **405**, 79-87.
6. Y. Yin, A. Sibley, J. S. Quinton, D. A. Lewis and G. G. Andersson, *Advanced Functional Materials*, 2018, **28**.
7. H. Shen, S. T. Omelchenko, D. A. Jacobs, S. Yalamanchili, Y. Wan, D. Yan, P. Phang, T. Duong, Y. Wu, Y. Yin, C. Samundsett, J. Peng, N. Wu, T. P. White, G. G. Andersson, N. S. Lewis and K. R. Catchpole, *Science Advance*, 2018, **4**, 9711.
8. C. J. P. A. Jablonski, *Journal of Electron Spectroscopy and Related Phenomena*, 1999, **100**, 137–160.
9. Y. Liu, G. Yin, W. An, Y. Ke and R. Quhe, *Nanotechnology*, 2022, **33**.
10. Y. Yin, D. A. Lewis and G. G. Andersson, *ACS Appl Mater Interfaces*, 2018, **10**, 44163-44172.
11. Y. Yin, X. Pan, M. R. Andersson, D. A. Lewis and G. G. Andersson, *ACS Applied Energy Materials*, 2019, **3**, 366-376.
12. S. Wang, Y. Xu, R. Chen, M. Zhu, M. Wang, M. Cao, Y. Liu, H. Ding, S. Zhang, J. Bai, J. Ren, T. Xuan and H. Li, *Coatings*, 2022, **12**.
13. X. Liu, S. Ren, Z. Li, J. Guo, S. Yi, Z. Yang, W. Hao, R. Li and J. Zhao, *Advanced Functional Materials*, 2022, **32**.
14. Y. Xie, B. Peng, I. Bravi´c, Y. Yu, Y. Dong, R. Liang, Q. Ou, B. Monserrat and S. Zhang, *Advanced Science News*, 2020, **7**, 2001698.
15. A. Sahai and N. Goswami, *Ceramics International*, 2014, **40**, 14569-14578.

16. N. Mozaffari, T. Duong, M. M. Shehata, A. D. Bui, H. T. Pham, Y. Yin, Y. O. Mayon, J. Zheng, M. A. Mahmud, G. D. Tabi, G. G. Andersson, L. E. Black, J. Peng, H. Shen, T. P. White, K. Weber and K. R. Catchpole, *Solar RRL*, 2022, **6**.
17. J. Endres, D. A. Egger, M. Kulbak, R. A. Kerner, L. Zhao, S. H. Silver, G. Hodes, B. P. Rand, D. Cahen, L. Kronik and A. Kahn, *J Phys Chem Lett*, 2016, **7**, 2722-2729; S. Tao, I. Schmidt, G. Brocks, J. Jiang, I. Tranca, K. Meerholz and S. Olthof, *Nat Commun*, 2019, **10**, 2560.
18. L. Yang, D. Li, C. Wang, W. Yao, H. Wang and K. Huang, *Journal of Nanoparticle Research*, 2017, **19**; F. Huang, L. Deng, T. Wang, A. Zhang, M. Yang and Y. Hou, *Mikrochim Acta*, 2023, **190**, 305.
19. R. T. Sapkal, S. S. Shinde, K. Y. Rajpure and C. H. Bhosale, *Journal of Semiconductors*, 2013, **34**.
20. W. Wisniewski, C. Genevois, E. Veron and M. Allix, *Powder Diffraction*, 2023, **38**, 139-144.